Chemical Engineering Journal 408 (2021) 127257

Contents lists available at ScienceDirect

Chemical Engineering Journal

journal homepage: www.elsevier.com/locate/cej

Anti-oxidative microstructure design of ultra-stable N-TiO_2 composite for the gaseous photodegradation reactions

Guanhong Lu, Xiao Wang, Yan Wang, Gansheng Shi, Xiaofeng Xie *, Jing Sun *

State Key Laboratory of High Performance Ceramics and Superfine Microstructure, Shanghai Institute of Ceramics, Chinese Academy of Sciences, 1295 Dingxi Road, Shanghai 200050, China

ARTICLE INFO

Keywords:
N-TiO_2@aTiO_2
CMS
Visible light
Photocatalytic activity
Acetaldehyde degradation

ABSTRACT

N doped TiO_2 has been extensively studied for its enhanced absorption to visible light and improved photocatalytic performance, however, its deactivation resulted from the loss of N caused by the oxidation effect is still a major obstacle in photocatalytic applications. In this work, N-TiO_2@aTiO_2 (N doped TiO_2 with amorphous TiO_2 layer on the surface) was prepared with the assistance of carbonaceous microsphere (CMS). Its photocatalytic activity in acetaldehyde degradation under visible light ($\lambda \geq 420$ nm) reached 25% and kept stable after 6 h, while N-TiO_2 began to deactivate after 80 min and completely lost its activity in the same conditions. Compared with N-TiO_2, almost no decrease in N content was observed in N-TiO_2@aTiO_2 due to the protective effect of TiO_2 amorphous layer. The electron spin-resonance (ESR) spectroscopy was further used to measure the variation tendency of N content with reaction time. The results reveal that TiO_2 amorphous layer effectively block the loss of N and prevent the deactivation of catalysts. This work provides a new approach to improve the stability of N-TiO_2 photocatalysts.

1. Introduction

Indoor air pollution has aroused people's widespread concern mainly because it causes serious health problems. Volatile organic compounds (VOCs) are the main indoor pollutants emitted from furniture, indoor decorations and so on [1–8]. Among various VOCs removal methods, photocatalysis has been widely studied as an efficient and low-cost green chemical technology, which can degrade organic pollutants under light at the room temperature. TiO_2 is widely applied in photocatalytic technologies due to its high chemical stability, non-toxicity and low cost [9–15]. However, pure TiO_2 can only absorb the ultraviolet light because of its wide band gap of 3.2 eV [16,17] and this limits its application for indoor air purification.

Many modification methods have been reported to increase the light absorption range of TiO_2, such as doping modification, semiconductor coupling, surface deposition modification and so on [18–21]. Among of them, nitrogen doping is a common and effective method to broaden the absorption range of TiO_2 [16,22–25]. N doped TiO_2 has been proven to be an effective photocatalyst for the photocatalytic oxidation (PCO) of organic pollutant under visible light irradiation [26–28]. However, N-TiO_2 has an inherent problem that it is prone to lose its photocatalytic activity because of the loss of N. Dong et al. [29] found that pure N-TiO_2 had an apparent decrease of photocatalytic activity for toluene degradation after four recycles under visible light, which was caused by the loss of N due to the oxidation of lattice-N by photogenerated holes. Villa et al. [30] proved that the deactivation of N-TiO_2 was mainly due to the leakage of N in the form of NH_4^+ during hydrogen production process under visible light irradiation.

To overcome this shortcoming, multiple modification methods have been reported to improve the stability of N-TiO_2. Chen et al. [31] discovered that annealing N-TiO_2 at 400 °C could improve the stability by stabilizing N atoms in the TiO_2 lattice. However, Dong et al. [29] reported that the loss of lattice-nitrogen still existed in N-TiO_2 prepared by partial oxidation of TiN powder at 400 °C for 2 h in the air. This meant that calcination may not be applicable to improve the stability of all N-TiO_2 materials prepared by different methods. Recently, some researchers used carbon materials to modify N-TiO_2 to improve its stability. Shao et al. [32] proved that C modified N-TiO_2 obtained with chitosan as a natural nitrogen and carbon source had better stability than N-TiO_2 in the cyclic photocatalytic degradation of Rh B. More recently, Huang et al. [33] prepared porous two-dimensional layered nitrogen-doped carbon-supported titanium dioxides (N-TiO_2@C)

* Corresponding authors.
E-mail addresses: xxfshcn@163.com (X. Xie), jingsun@mail.sic.ac.cn (J. Sun).

https://doi.org/10.1016/j.cej.2020.127257
Received 13 June 2020; Received in revised form 3 September 2020; Accepted 2 October 2020
Available online 8 October 2020

derived from Ti_3C_2 MXene, which remained good photocatalytic activity for phenol degradation after 10 times cycle tests under visible light. However, the reported work did not explain the mechanism of C-modification for improving the stability of N-TiO_2 or inhibiting the loss of N.

In this work, nitrogen doped TiO_2 coated with TiO_2 amorphous layer (N-TiO_2@aTiO_2) was synthesized through hydrothermal process in the presence with carbonaceous microsphere (CMS). Element quality content testing and electron spin-resonance (ESR) spectroscopy were both used to detect the variation of N content with reaction time. Compared to N-TiO_2, N-TiO_2@aTiO_2 showed highly improved stability in photocatalytic degradation of acetaldehyde under visible light. The possible mechanism for the high stability of N was proposed. This work can provide a new method to enhance the service life of N-TiO_2 and promote its application in photocatalytic degradation of organic pollutant.

2. Experimental section

2.1. Materials preparation

All the chemicals are commercially available and used as received without any further purification. They are tetrabutyl titanate ($C_{16}H_{36}O_4Ti$, AR, 98%, Sinapharm Chemical Reagent Co., Ltd, China), nitric acid (HNO_3, AR,65 ~ 68%, Sinapharm Chemical Reagent Co., Ltd, China), urea (CH_4N_2O, AR, 99.7%, Zhenxing No.1 Chemical Plant, China), ethanol (C_2H_6O, AR, 99.7%, Zhenxing No.1 Chemical Plant, China) and glucose ($C_6H_{12}O_6$, AR, 97%, Sinapharm Chemical Reagent Co., Ltd, China).

2.2. Preparation of the carbonaceous microsphere (CMS)

CMS was prepared via the polymerization emulsification of sucrose according to literatures [34,35]. In a typical preparation process, 26 g glucose was dissolved in 50 mL deionized water and sealed in a 100 mL Teflon autoclave, followed by hydrothermal treatment for 6 h at 160 °C. The obtained black powder was collected and washed twice with deionized water and ethanol separately. The powder was then dried in a drying oven at 70 °C for 2 h and stored in a desiccator.

2.3. Preparation of N-TiO_2@aTiO_2

The CMS assisted N-doped TiO_2 powder was synthesized via sol–gel method. 6.6 g urea was dissolved into 100 mL 95% ethanol to obtain solution A. 0.3 g CMS was dispersed in 100 mL ethanol and mixed with 0.5 mL 65 ~ 68% nitric acid and 25 mL tetrabutyl titanate to get solution B. Then solution A was dropwise added into solution B under vigorous stirring and stored in a fume cupboard. The as-prepared gel was dispersed into 250 mL DI water and sealed in Teflon autoclave and hydrothermally treated at 180 °C for 6 h. The precipitate was centrifugated and washed twice with deionized water and ethanol before being dried at 80 °C. Finally, the black powder was calcined at 400 °C for 1 h and was named as N-TiO_2@aTiO_2. For comparison, pure TiO_2 was prepared by the same procedure without CMS and urea. Sample TiO_2@aTiO_2 (TiO_2 coated by TiO_2 amorphous layer) was prepared in presence of CMS. N-doped TiO_2 (N-TiO_2) was prepared with urea without CMS. The process was shown in scheme 1.

2.4. Materials characterizations

The crystalline structure of the photocatalysts was investigated by X-ray diffractometer (XRD; Ultima IV 2036E102, Rigaku Corporation, Japan) with Cu Kα radiation at 50 Hz at the rate of 10°/min. The surface morphology and microstructure of the materials was measured by a field-emission scanning electron microscope (SEM; SU8220, Hitachi, Japan) and a transmission electron microscope (TEM; JEM-2100F, JEOL, Japan) with electron energy loss spectroscopy (EELS). Raman spectroscopy was carried out on the DXR Raman Microscope (Thermo-Fisher Scientific, USA) from 65 to 1000 $cm^{-1}$with a 532 nm excitation wavelength. The specific surface area of the photocatalysts was analyzed by Brunauer, Emmett and Teller (BET) nitrogen sorption surface area measurements, using an analyzer (Micromeritics ASAP 3000 system, Micromeritics, USA). X-ray photoelectron spectra (XPS) was obtained on a spectrometer (Microlab 310F Scanning Auger Microprobe, VG SCIENTIFIC LTD) with a constant pass energy of 50 eV by a monochromatic Al-Ka (1486.6 eV) X-ray. The optical absorption properties of the photocatalysts were measured by a UV–Vis spectrophotometer (Lambda 950 UV/Vis spectrometer, Perkin Elmer, USA). The contents of nitrogen and carbon elements were determined by a nitrogen-carbon detector (Multi N/C® 3100, Analytik Jena AG, Germany). Electron spin-resonance spectroscopy (ESR, JEOL-FA200, Japan) was used to probe the paramagnetic nitrogen species in this work.

2.5. Radical detection

Hydroxyl radical (·OH) and superoxide radical ($\cdot O_2^-$) were also studied by ESR with 5,5-dimethyl-1-pyrroline-N-oxide (DMPO) as a

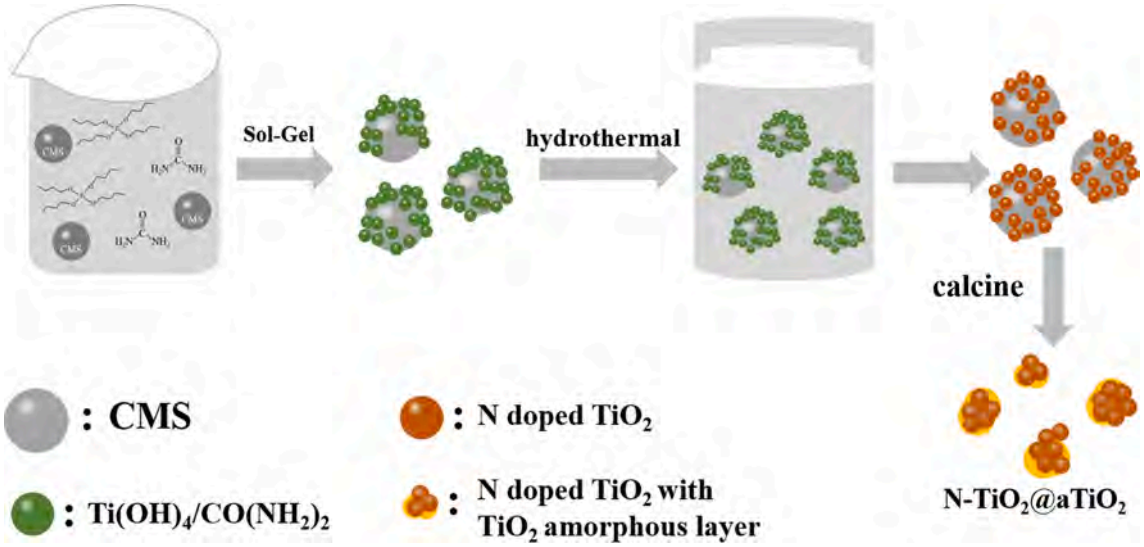

Scheme 1. The schematic diagram of the preparation process of N-TiO_2@aTiO_2.

capture agent. Generally, ·OH and $\cdot O_2^-$ were detected in water and ethanol, respectively. 50 mg photocatalyst was dispersed in 10 mL water or ethanol and subsequently ultrasonicated for 15 min to obtain solution C. 4 μL DMPO was added to a 1 mL sample cell containing 100 μL of solution C, then the mixed solution was used to detect the radicals by an electron spin-resonance spectroscope (ESR, JEOL-FA200, Japan).

2.6. Photoelectric performance test

Photo-current response of the as-prepared samples were measured by a CHI660D electrochemical workstation [36]. 0.2 g photocatalyst powder was added into 6 mL ethanol to prepare the paste by the wet milling method. The paste was then spin-coated on FTO substrate with the speed of 2000 r/min to gain the work electrode. The effective spin-coating area was 1 cm × 1.5 cm. The light irradiation source was a 400 W Xe lamp with a 420 nm cut-off filter ($\lambda \geq 420$ nm). In photocurrent test, the photocatalyst/FTO as the work electrode along with a platinum plate and an Ag/AgCl electrode as the counter and reference electrodes was put into 1 mol/L NaCl to constitute a three-electrode system under the "i-t curve" test mode on the electrochemical workstation.

2.7. Photocatalytic performance test

The photocatalytic performance of the sample was tested in a continuous flow reactor system. The schematic diagram of this reactor was showed in Fig. S1. 0.1 g photocatalyst was milled in ethanol and then coated on a 7.5 cm × 15 cm glass pane. It was dried at 80 °C for 1 h in the oven to remove ethanol. Then the glass pane was put into the reaction chamber with a transparent quartz cover. 1000 ppm acetaldehyde with a flow rate of 10 mL/min was diluted with high purity air of the same flow rate to 500 ppm. The high purity air passed through the humidifying tank to carry moisture which will participate in the photocatalytic reaction process. The acetaldehyde concentration was tested directly by gas chromatography (GC7920, Beijing China Education Au-Light Co., Ltd., China). The mixed gas containing 500 ppm acetaldehyde passed through the photocatalyst at a flow speed of 20 mL/min and the light was turned on after the adsorption equilibrium reached. 400 W Xe lamp with a 420 nm cut-off filter was used as the visible light irradiation source, which was placed 20 cm above the photocatalysts. The dark adsorption process was taken place at room temperature (25 °C), while the temperature of the sample surface would reach and stay at about 55 °C due to the irradiation of the xenon lamp in the photocatalytic process.

C_0 and C are the initial concentration and the real-time concentration of acetaldehyde during the photocatalytic reaction, respectively. C/C_0 was used to evaluate acetaldehyde removal performance of photocatalysts under visible light.

3. Results and discussions

The SEM morphology images of TiO_2, TiO_2@aTiO_2, N-TiO_2 and N-TiO_2@aTiO_2 were shown in Fig. 1a-d. TiO_2 particles all agglomerated in four samples. Particle size of TiO_2 ranged from 12 to 22 nm as show in Fig. 1a and the boundary between particles was clear. Compared with pure TiO_2, particle size decreased to around 10 nm for the other three samples. The SEM image of N-TiO_2@aTiO_2 is rather blurry, and the interface between particles are not clear. The samples were observed by high-resolution transmission electron microscope (HRTEM) as shown in Fig. 2. Fig. 2a- Fig. 2c were the HRTEM images of N-TiO_2 and Fig. 2d-Fig. 2f were for N-TiO_2@aTiO_2. The lattice stripes traversed the entire

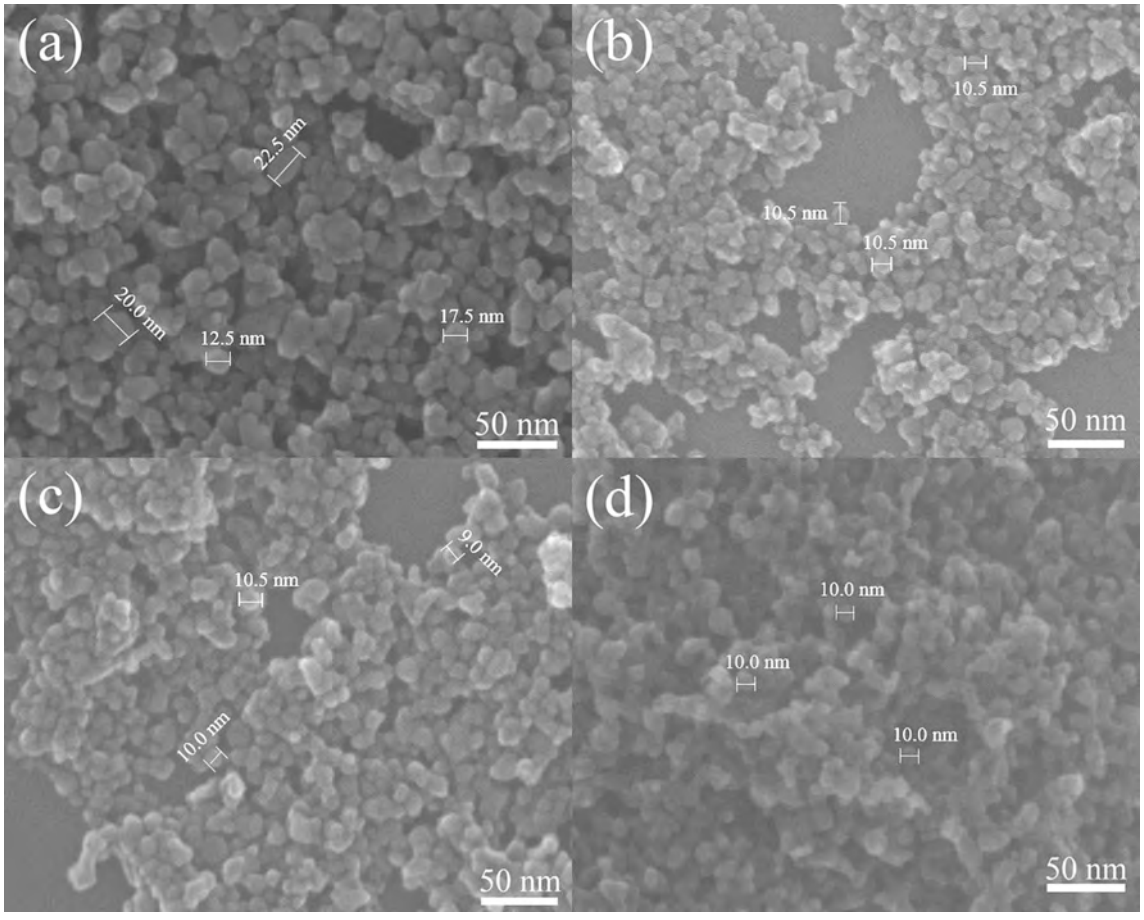

Fig. 1. SEM images of (a) TiO_2, (b) TiO_2@aTiO_2, (c) N-TiO_2, (d) N-TiO_2@aTiO_2.

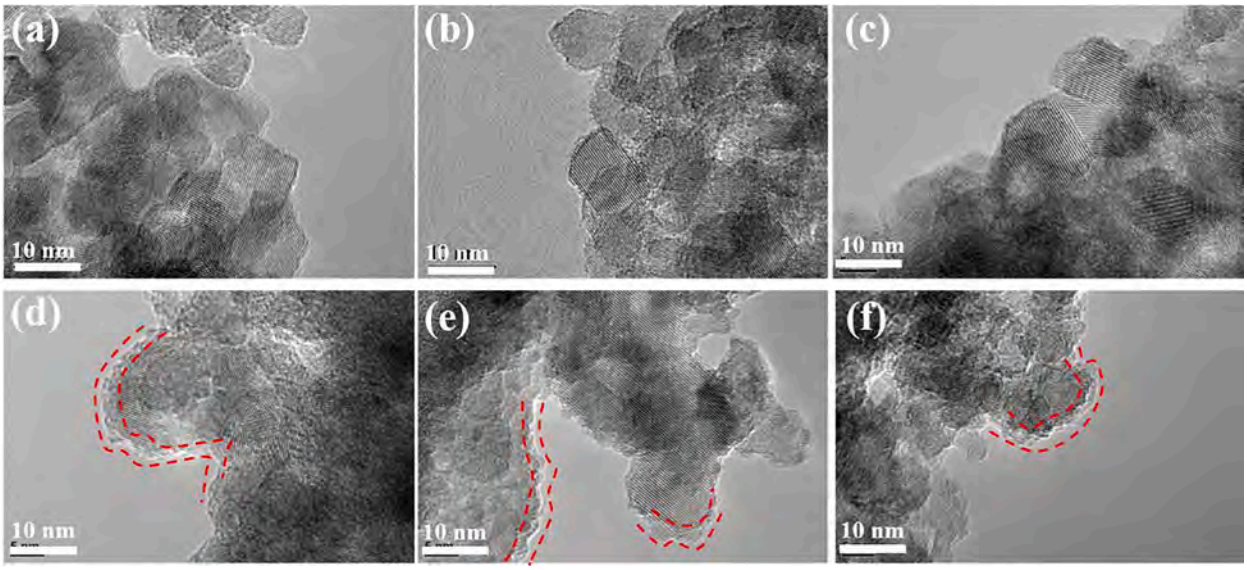

Fig. 2. HRTEM images of (a-c) N-TiO_2 and (d-f) N-TiO_2@aTiO_2.

particle and was distinct at the edges of particles in N-TiO_2. However, the lattice fringe became fuzzy at the edges in N-TiO_2@aTiO_2 and obvious amorphous layer (as indicated by the red dotted line) could be observed. XRD patterns are shown in Fig. 3. The half peak widths of TiO_2, TiO_2@aTiO_2, N-TiO_2 and N-TiO_2@aTiO_2 were 0.605°, 0.786°, 0.757° and 0.784°, respectively. The larger half-peak width means the smaller particle size according to Scherrer equation [37]. The crystals structure in all four samples contained both anatase and brookite phase corresponding to PDF#21–1272 and PDF#29–1360, respectively. The above result showed that the introduction of urea and CMS had almost no influence on the crystalline structure of TiO_2 but decreased the particle size obviously.

To further analyze the composition of the amorphous layer, the content of nitrogen and carbon were measured and the mass percentage for C and N were about 0.214 wt% and 0.155 wt% in N-TiO_2@aTiO_2, respectively. The C mass percentage decayed from 5 wt% (the addition amount) to 0.214 wt% after being calcinated. DXR Raman spectra of as-prepared photocatalysts were measured in Fig. 4a. There were four distinct characteristic peaks at 144 cm^{-1}, 398 cm^{-1}, 516 cm^{-1} and 638 cm^{-1}, which corresponded to the E_g, B_{1g}, A_{1g} and B_{2g} vibrational modes

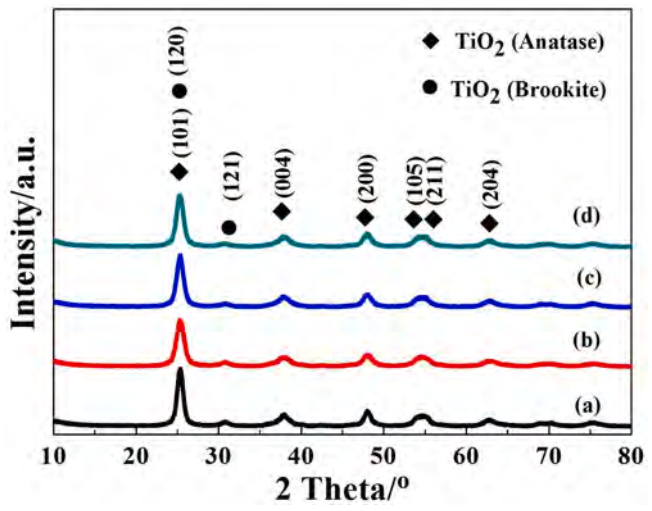

Fig. 3. XRD patterns of (a) TiO_2, (b) TiO_2@aTiO_2, (c) N-TiO_2 and (d) N-TiO_2@aTiO_2.

of anatase TiO_2, respectively. No obvious Raman peaks of carbon at 1346 cm^{-1} and 1560 cm^{-1} [38] were observed in both of TiO_2@aTiO_2 and N-TiO_2@aTiO_2 (Fig. S2), proving that the most CMS was removed after calcination at 400 °C. N-TiO_2@aTiO_2 was further characterized by EELS and TEM. As shown in Fig. 4b, one region with a diameter of about 200 nm (1 #) and single particle surface (2 #) were selected for EELS analysis, typical element peaks of Ti and O appeared. Since no obvious C peak at 283 eV were observed both in Fig. 4c and Fig. 4d, thin amorphous layer on the surface of N-TiO_2@aTiO_2 was TiO_2. It formed in calcination process with presence of CMS, which inhibited the transition of amorphous TiO_2 to anatase TiO_2.

Fig. 5 presented Ti 2p and N 1 s XPS spectra of N-TiO_2@aTiO_2. The peaks of Ti 2p1/2 and Ti 2p3/2 of N-TiO_2@aTiO_2 were located at 464.3 eV and 458.7 eV in Fig. 5a, respectively, which were assigned to typical TiO_2 [39,40]. The N1s XPS spectrum of N-TiO_2@aTiO_2 was showed in Fig. 5b. The characteristic peak at about 400.3 eV was namely interstitial N atoms, where N atoms bound to O lattice atoms to form Ti-O-N [41–43]. The N 1 s peak at about 396.9 eV was generally corresponding to N–Ti–N bonds resulting from the nitrogen atoms replacing O lattice atoms in the TiO_2 crystal lattice, which was named as substitutional N atoms [44,45].

To evaluate the performance of as-prepared photocatalysts, photocatalytic degradation for acetaldehyde was performed in a continuous flow reactor system under visible light (Fig. 6). Fig. 6a and Fig. 6b were the adsorption equilibrium curves in dark and acetaldehyde degradation curves under visible light, respectively. Acetaldehyde desorption occurred in the initial stage of photocatalytic reaction due to the thermal effect xenon lamp, which made C/C_0 greater than 1 in the first 30–40 min. The photocatalytic degradation efficiency of pure TiO_2 reached 5.6% at about 80 min after turning on the light. However, it began to deactivate afterwards and then was completely deactivated after 200 min. Subsequently, C/C_0 value of TiO_2 was greater than 1. The reason was the adsorbed acetaldehyde continued to desorb from the surface of catalyst after the complete deactivation of TiO_2. The photocatalytic degradation efficiency of TiO_2@aTiO_2 is about 4% under visible light irradiation and the performance maintained during photocatalysis. The enhanced visible photocatalytic degradation properties of N-TiO_2 and N-TiO_2@aTiO_2 was observed as compared to TiO_2 and TiO_2@aTiO_2, indicating the significant role of N doping. The photocatalytic degradation rate of N-TiO_2 was faster than that of N-TiO_2@aTiO_2 in the first 90 min after turning on the light. However, N-TiO_2 began to deactivate after 2 h and was completely deactivated in about 6 h, while N-

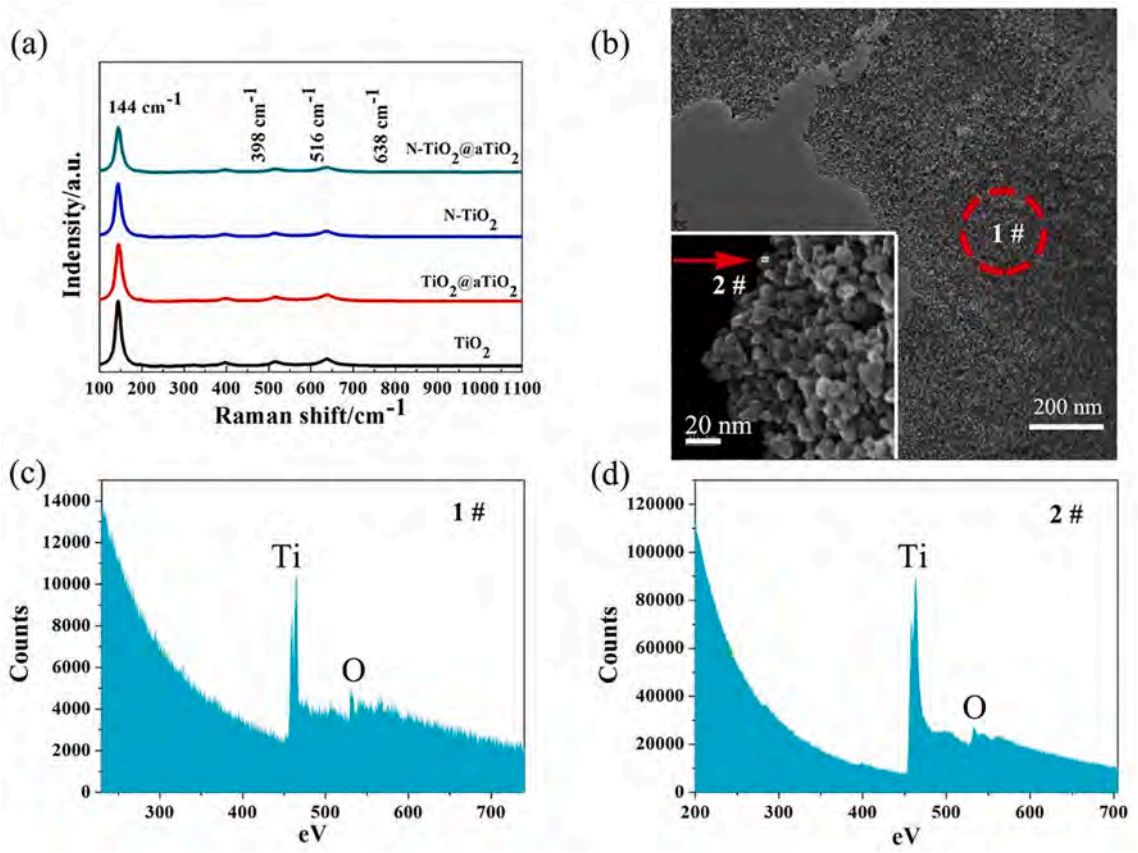

Fig. 4. (a) Raman data of the as-prepared photocatalysts; (b) TEM image of N-TiO_2@aTiO_2; (c-d) EELS spectra for N-TiO_2@aTiO_2 corresponding to the two regions marked in (b).

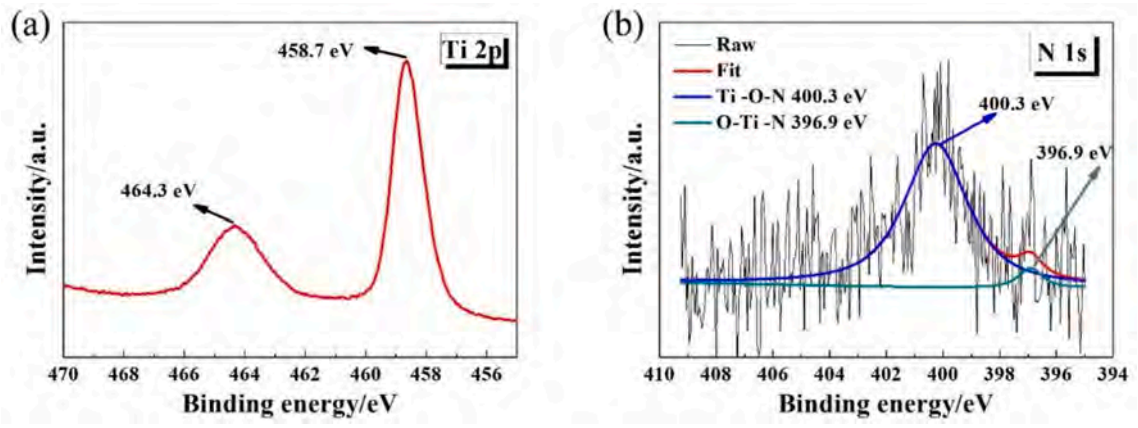

Fig. 5. (a) Ti 2p and (b) N 1 s XPS spectra of N-TiO_2@aTiO_2.

TiO_2@aTiO_2 maintained good photocatalytic activity within 6 h with photo degradation efficiency of 25%.

To further verify this finding about the stability of N-TiO_2@aTiO_2, the acetaldehyde photocatalytic degradation tests of N-TiO_2 and N-TiO_2@aTiO_2 were also performed without water (0% RH condition). N-TiO_2 was completely deactivated after 250 min irradiation in the absence of water as showed in Fig. S3. The deactivated rate became much faster than that in the presence of water. N-TiO_2@aTiO_2 maintained excellent photocatalytic stability as well under anhydrous condition.

To better understand the result of photocatalytic degradation of acetaldehyde, more experimental data would be provided as follows. The specific surface area (SSA) of as-prepared photocatalysts was calculated using the Brunauer–Emmett–Teller (BET) method. As listed in Table 1, the SSA of TiO_2, TiO_2@aTiO_2, N-TiO_2 and N-TiO_2@aTiO_2 was 102.7 m^2/g, 118.0 m^2/g, 134.5 m^2/g and 142.4 m^2/g, respectively. The particle sizes of four samples calculated according to the half-peak width and Scheler's formula were also listed in Table 1. Obviously, CMS and urea could both inhibit TiO_2 crystallite growth to further increase the SSA. N-TiO_2@aTiO_2 had a largest SSA under the combined effects of CMS and N doped.

In order to further test the adsorption behavior of acetaldehyde on different photocatalysts, the temperature programmed desorption (TPD) was detected. As shown in Fig. S4, all four samples showed two peaks at

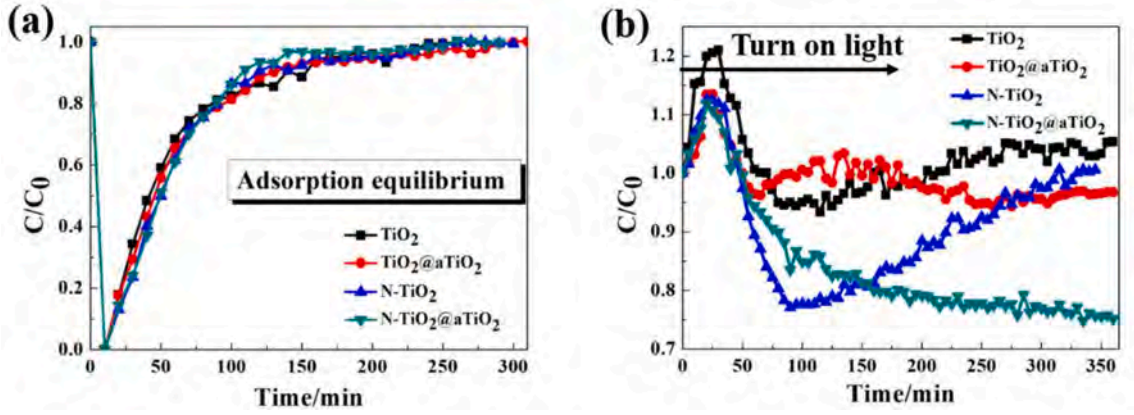

Fig. 6. (a) Dark adsorption curves of four samples; (b) Degradation of acetaldehyde on four samples under visible light.

Table 1
The particle sizes and specific surface area (SSA) of as-prepared photocatalysts.

Sample	Particle sizes/ nm	SSA/ m^2/g
TiO_2	13.3	102.7
TiO_2@aTiO_2	10.2	118.0
N-TiO_2	10.6	134.5
N-TiO_2@aTiO_2	10.3	142.4

similar desorption temperature at about 270 °C and 500 °C, which manifested that there were two adsorption modes between acetaldehyde and the as-prepared photocatalysts. N-TiO_2@aTiO_2 showed the highest intensity of the desorption peak at 500 °C, indicating it had higher adsorption capacity of acetaldehyde, which can be ascribed to its larger SSA among the four photocatalysts.

The light absorption spectra of photocatalysts in the wavelength range of 250–800 nm was shown in Fig. 7a. Compared to pure TiO_2, N-TiO_2 had a more absorption in the visible region from 400 nm to 500 nm, which was consistent with the previous reported work [46]. Similarly, N-TiO_2@aTiO_2 also had a higher visible light absorption intensity than N-TiO_2. Therefore, N doping and the introduction of the CMS could both enhance the light absorption in the visible range. According to Kubelka Munk, the bandgap values of TiO_2, TiO_2@aTiO_2, N-TiO_2 and N-TiO_2@aTiO_2 were 2.90 eV, 2.80 eV, 2.85 eV and 2.77 eV, respectively (see in Fig. S5). The band gap of pure TiO_2 is only 2.9 eV (less than 3.2 eV), which may be caused by the formation of brookite TiO_2. The bandgap of pure brookite TiO_2 was about 2.0 eV [47].

Photocurrent test was carried out to further study the effect of TiO_2 amorphous on N-TiO_2@aTiO_2 for the separation of photogenerated electron-hole pairs. TiO_2@aTiO_2 had a slightly higher photocurrent than TiO_2 under visible light, which may be resulted from the fact that the visible light absorption intensity of TiO_2@aTiO_2 was stronger than that of pure TiO_2 as shown in Fig. 7a. The photocurrent intensity of N-TiO_2@aTiO_2 decreased gradually and was completely lower than that of N-TiO_2 after the five cycle tests. The possible reason was that the amorphous TiO_2 on the surface of N-TiO_2@aTiO_2 played the role as defects and captured the photogenerated electron hole pairs, thus lead to the decease on photocurrent [48]. In addition, the photocurrent of N-TiO_2@aTiO_2 was higher than that of TiO_2@aTiO_2, manifesting that the visible light response was mainly contributed by N doping. This result was consistent with the photocatalytic degradation result (see in Fig. 6).

Although N-TiO_2 had the higher photocurrent than N-TiO_2@aTiO_2, it was easy to be deactivated in photocatalytic degradation of acetaldehyde. To further study the deactivation of N-TiO_2, N element mass percentage of N-TiO_2 and N-TiO_2@aTiO_2 were measured before and after the photocatalytic reaction (As shown in Table 2). The content of N element decreased from 0.163 wt% to 0.062 wt% in N-TiO_2, while only a slight decrease of N mass from 0.155 wt% to 0.147 wt% was observed for N-TiO_2@aTiO_2. Therefore, it was believed that the main reason for the deactivation of N-TiO_2 was caused by the loss of N element in the photocatalytic reaction.

In order to better investigate the process of N element loss in photocatalytic reaction, ESR tests were carried out at different

Table 2
N element mass percent of N-TiO_2 and N-TiO_2@aTiO_2 was tested before and after the photocatalytic reaction.

	as-prepared	after photodegradation
N-TiO_2@aTiO_2	0.155 wt%	0.147 wt%
N-TiO_2	0.163 wt%	0.062 wt%

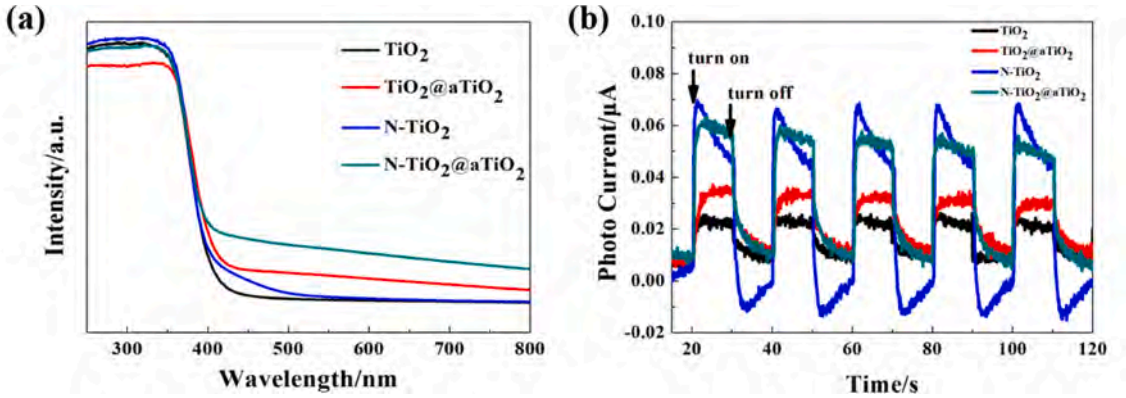

Fig. 7. (a) UV–Vis diffuse reflectance spectra of as-prepared photocatalysts; (b) Photocurrent test of the photocatalysts under visible light.

photocatalytic reaction time. According to the literature [49], ESR signal peaks with spin Hamiltonian parameters (g = 2.004, A = 3.26 mT in Fig. 8a and g = 2.003, A = 3.24 mT in Fig. 8b) were ascribed to N species in N-TiO_2 and N-TiO_2@aTiO_2, respectively. N atoms has two types of localized energy states in N-doped TiO_2 material both on the basis of experimental evidences [50,51] and rigorous quantum chemical calculation [52,53]. The two localized energy states correspond to two different N atoms bonding types, one is substitutional N atoms and another is interstitial N atoms. The XPS results also provided evidences for the existence of these two N species. The two N species cannot be distinguished on the ESR signal because they are both paramagnetic. As shown in Fig. 8a and 8b, in the first 2 h of photocatalytic reaction, the peak intensity of N species decreased rapidly both in N-TiO_2 and N-TiO_2@aTiO_2. The interstitial N atoms bond with lattice O to form interstitials species, which can be described a true π radical ion NO^{2-}. NO^{2-} could get photogenerated electrons from photocatalyst under visible light to form diamagnetic (ESR silent) species (NO^{3-}) [43]. This may be the main reason for the rapid decline of ESR signal intensity of N species. Remarkably, the ESR peak intensity of N-TiO_2@aTiO_2 remained unchanged from the 2nd hour to the 6th hour of the photocatalytic reaction, while that of N-TiO_2 continued to decline (as shown in Fig. 8c-Fig. 8f). This result indicated that the N loss in N-TiO_2 was a continuous process under visible light. According to the previous work [29,31], the loss of lattice N was mainly due to its oxidization by photogenerated holes, which was the possible reason for the continuous loss of N in N-TiO_2 in this work. As for N-TiO_2@aTiO_2, defects in amorphous TiO_2 captured the photogenerated electrons and holes and inhibited the oxidation of lattice N by holes.

ESR was used to measure the intensity of ·OH and·O_2^- as shown in Fig. 9a and 9b. The four ESR signal peaks with the intensity ratio of 1:2:2:1 and six characteristic peaks corresponded to ·OH and·O_2^-, respectively [54,55]. The signal intensity of ·OH for N-TiO_2@aTiO_2 and N-TiO_2 were almost overlapped, while the signal intensity of ·O_2^- for N-TiO_2@aTiO_2 was higher than that of N-TiO_2. This result indicated that

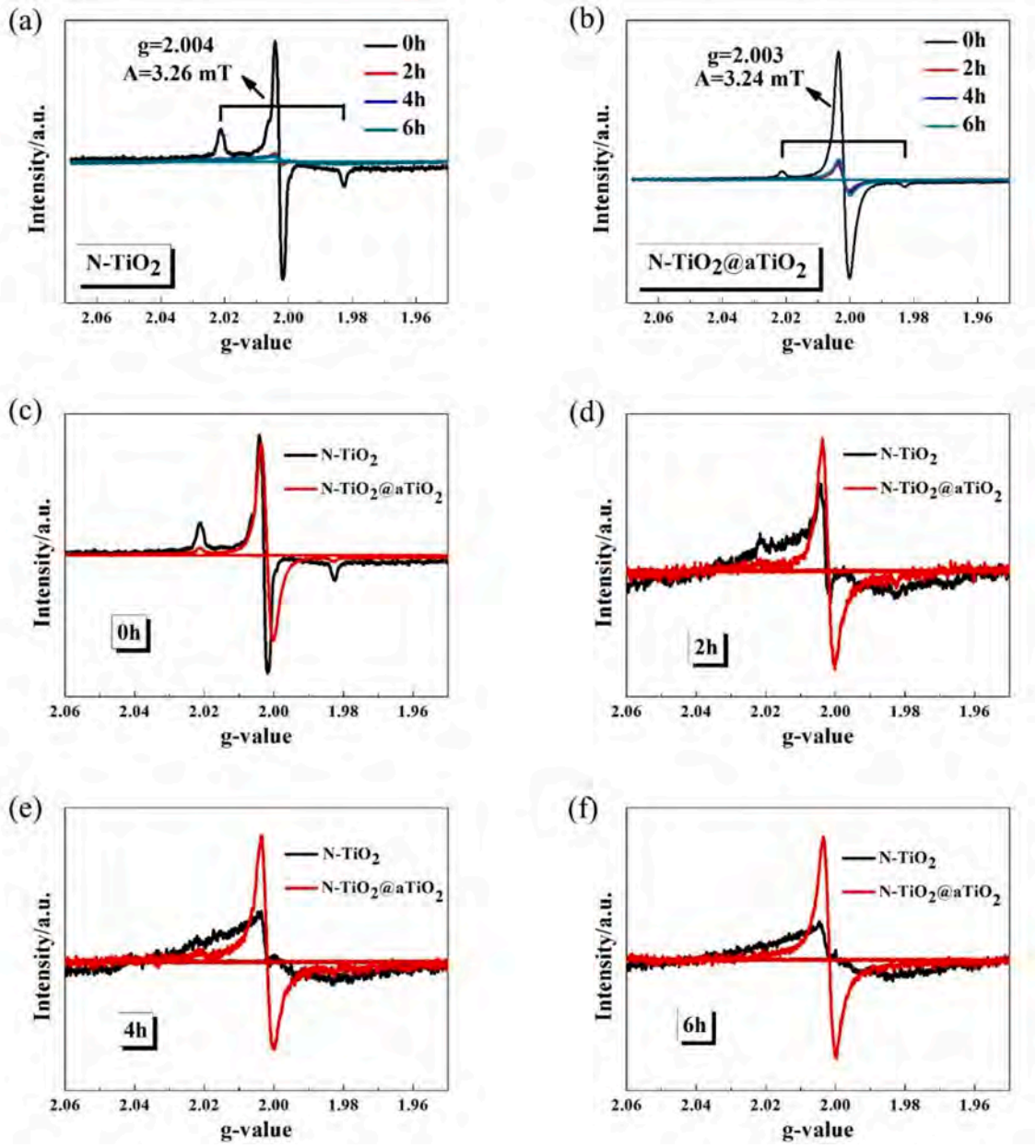

Fig. 8. ESR spectra of (a) N-TiO_2 and (b) N-TiO_2@aTiO_2 at the different reaction time in photocatalytic degradation for acetaldehyde; c-d: ESR comparison results of N-TiO_2 and N-TiO_2@aTiO_2 after same reaction times (c: at 0 h; d: at 2nd hour; e: at 4th hour; d: 6th hour).

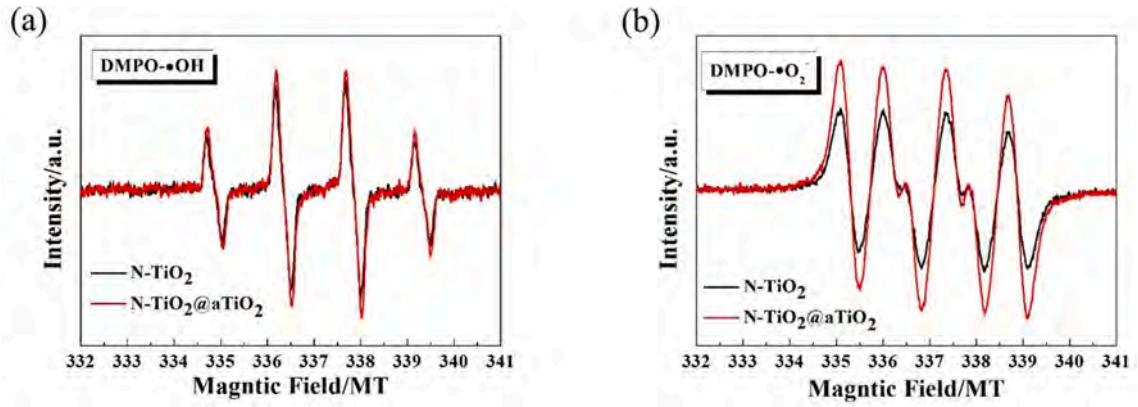

Fig. 9. Radical analysis on N-TiO_2 and N-TiO_2@aTiO_2 under visible light (a: DMPO-●OH; b: DMPO-●O_2^-).

N-TiO_2@aTiO_2 absorbed more O_2 molecules, which could be ascribed to the amorphous TiO_2 layer played a role on it.

Typically, the loss of lattice N occurred due to its being oxidized by the photogenerated holes [29,31]. In the reaction process, O atoms would replace lattice N to reconstruct TiO_2 crystal lattice. According to photocurrent and ESR radical results, the possible mechanism for the amorphous TiO_2 inhibiting N loss in photocatalysis process was proposed as shown in Scheme 2. First, the defects in amorphous TiO_2 were prone to capture photogenerated electron hole pairs and the oxidation of lattice N by holes was effectively inhibited. Secondly, the amorphous TiO_2 layer with oxygen vacancy defects was prone to adsorb oxygen-containing molecules. Thus, O_2 would be prevented from entering into N-TiO_2 and the loss of N was prevented.

4. Conclusions

In summary, N doped TiO_2 with amorphous TiO_2 layer on the surface (N-TiO_2@aTiO_2) has been successfully synthesized by introducing carbonaceous microsphere (CMS). The photocatalytic activity of N-TiO_2@aTiO_2 reached 25% and still maintained active after 6 h acetaldehyde degradation under visible light ($\lambda \geq 420$ nm), while N-TiO_2 began to deactivate after 80 min and completely lost its activity in the same conditions. The excellent photocatalytic stability of N-TiO_2@aTiO_2 was ascribed to the positive effect of the TiO_2 amorphous layer, which effectively inhibited the loss of doping N as evidenced by the N element content test and ESR. The content of N element decreased from 0.155 wt % to 0.147 wt% in N-TiO_2@aTiO_2, while a high decrease of N mass from 0.163 wt% to 0.062 wt% was observed for N-TiO_2. The essential mechanisms have been proposed that amorphous TiO_2 could capture the photogenerated electron hole pairs and adsorb O_2, thus inhibiting the

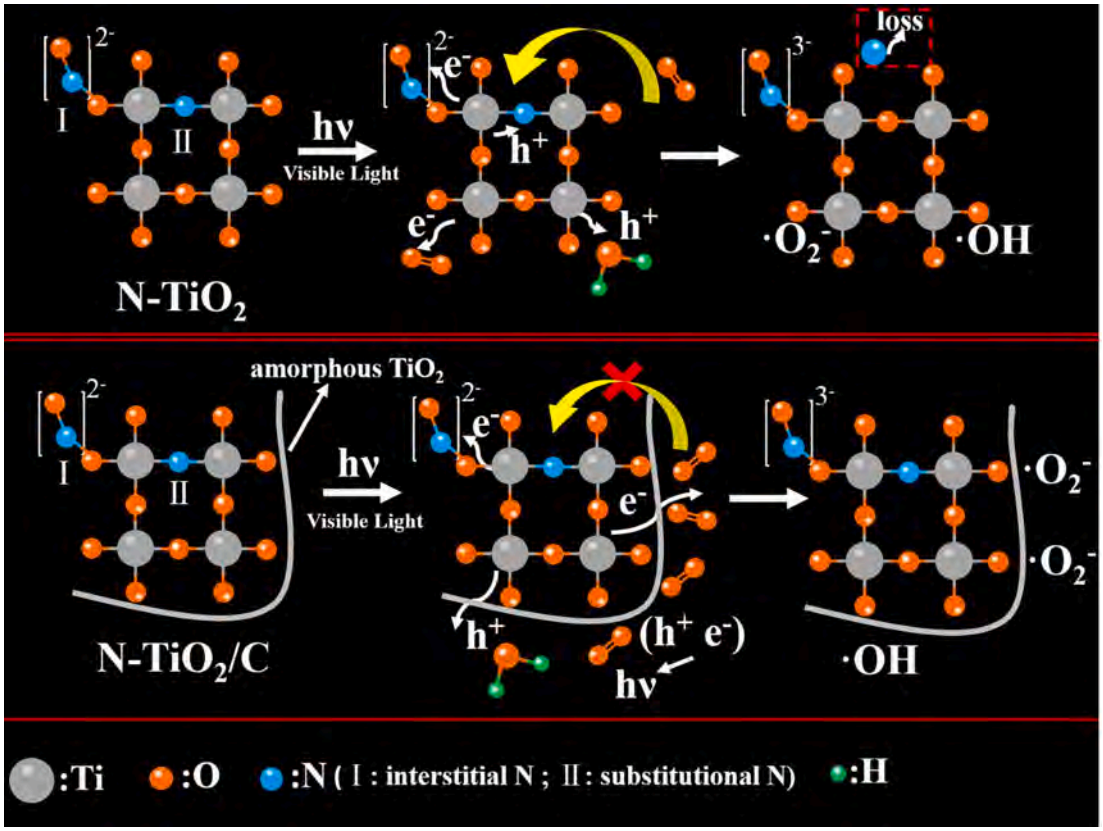

Scheme 2. Mechanism diagram of inhibiting N loss by amorphous TiO_2.

oxidation reaction of lattice nitrogen. This work provides a new way to improve the stability of N-TiO_2 photocatalysts and promotes its long-term application.

Declaration of Competing Interest

The authors declare that they have no known competing financial interests or personal relationships that could have appeared to influence the work reported in this paper.

Acknowledgements

This work was financially supported by the National Key Research and Development Program of China (2016YFA0203000), Shanghai Commission of Science and Technology Program (19DZ1202600, 20DZ1204100), the National Natural Science Foundation of China (Grant No. 41907303), the Innovation Fund of SICCAS (Y91ZC5150G).

Appendix A. Supplementary data

Supplementary data to this article can be found online at https://doi.org/10.1016/j.cej.2020.127257.

References

[1] B.R. Raju, E.L. Reddy, J. Karuppiah, P.M.K. Reddy, C. Subrahmanyam, Catalytic non-thermal plasma reactor for the decomposition of a mixture of volatile organic compounds, J. Chem. Sci. 125 (2013) 673–678.
[2] T. Tabakova, D. Dimitrov, M. Manzoli, F. Vindigni, P. Petrova, L. Ilieva, R. Zanella, K. Ivanov, Impact of metal doping on the activity of Au/CeO_2 catalysts for catalytic abatement of VOCs and CO in waste gases, Catal. Commun. 35 (2013) 51–58.
[3] Z.-L. Que, F.-B. Wang, J.-Z. Li, T. Furuno, Assessment on emission of volatile organic compounds and formaldehyde from building materials, Compos. B Eng. 49 (2013) 36–42.
[4] M. Hinojosa-Reyes, S. Arriaga, L.A. Diaz-Torres, V. Rodríguez-González, Gas-phase photocatalytic decomposition of ethylbenzene over perlite granules coated with indium doped TiO_2, Chem. Eng. J. 224 (2013) 106–113.
[5] L. Jiang, H. Li, J. Chen, D.i. Zhang, S. Cao, J. Ye, Combination of non-thermal plasma and biotrickling filter for chlorobenzene removal: The NTP combined with BTF system, J. Chem. Technol. Biotechnol. 91 (12) (2016) 3079–3087.
[6] J. Chen, X.i. Chen, W. Xu, Z. Xu, J. Chen, H. Jia, J. Chen, Hydrolysis driving redox reaction to synthesize Mn-Fe binary oxides as highly active catalysts for the removal of toluene, Chem. Eng. J. 330 (2017) 281–293.
[7] C.-S. Lee, Z. Dai, D.H. Kim, H.-Y. Li, Y.-M. Jo, B.-Y. Kim, H.-G. Byun, I. Hwang, J.-H. Lee, Highly discriminative and sensitive detection of volatile organic compounds for monitoring indoor air quality using pure and Au-loaded 2D In_2O_3 inverse opal thin films, Sens. Actuators. B: Chem. 273 (2018) 1–8.
[8] X.i. Chen, X.i. Chen, S. Cai, E. Yu, J. Chen, H. Jia, MnOx/Cr_2O_3 composites prepared by pyrolysis of Cr-MOF precursors containing in situ assembly of MnOx as high stable catalyst for toluene oxidation, Appl. Surf. Sci. 475 (2019) 312–324.
[9] W.-T. Chen, A. Chan, D. Sun-Waterhouse, T. Moriga, H. Idriss, G.I.N. Waterhouse, Ni/TiO2: A promising low-cost photocatalytic system for solar H2 production from ethanol–water mixtures, J. Catal. 326 (2015) 43–53.
[10] I. Cimieri, H. Poelman, N. Avci, J. Geens, S.D. Lambert, B. Heinrichs, D. Poelman, Sol–gel preparation of pure and doped TiO_2 films for the photocatalytic oxidation of ethanol in air, J Sol-Gel Sci Technol 63 (3) (2012) 526–536.
[11] M. Luna, J.M. Gatica, H. Vidal, M.J. Mosquera, Au-TiO_2/SiO_2 photocatalysts with NO_x depolluting activity: Influence of gold particle size and loading, Chem. Eng. J. 368 (2019) 417–427.
[12] D. Wang, L. Xiao, Q. Luo, X. Li, J. An, Y. Duan, Highly efficient visible light TiO_2 photocatalyst prepared by sol-gel method at temperatures lower than 300 ^{o}C, J. Hazard. Mater. 192 (2011) 150–159.
[13] A.K.L. Sajjad, S. Shamaila, B. Tian, F. Chen, J. Zhang, One step activation of WO_x/TiO_2 nanocomposites with enhanced photocatalytic activity, Appl. Catal. B: Environ. 91 (2009) 397–405.
[14] S. Qourzal, N. Barka, M. Tamimi, A. Assabbane, Y. Ait-Ichou, Photodegradation of 2-naphthol in water by artificial light illumination using TiO_2 photocatalyst: Identification of intermediates and the reaction pathway, Appl. Catal. A: Gen. 334 (2008) 386–393.
[15] S.-D. Yoon, E.-S. Kim, Y.-H. Yun, Chemical durability and photocatalyst activity of acid-treated ceramic TiO_2 nanocomposites, J. Ind. Eng. Chem. 64 (2018) 230–236.
[16] J.-H. Xu, W.-L. Dai, J. Li, Y. Cao, H. Li, H. He, K. Fan, Simple fabrication of thermally stable apertured N-doped TiO_2 microtubes as a highly efficient photocatalyst under visible light irradiation, Catal. Commun. 9 (1) (2008) 146–152.
[17] C. Gao, T. Wei, Y. Zhang, X. Song, Y. Huan, H. Liu, M. Zhao, J. Yu, X. Chen, A Photoresponsive Rutile TiO_2 Heterojunction with Enhanced Electron-Hole Separation for High-Performance Hydrogen Evolution, Adv. Mater. 31 (2019) e1806596.
[18] X. Liu, L.-J. Chen, R.-Y. Chen, Z. Chen, X. Chen, X.i. Zheng, Preparation and characterization of bipolar membranes modified by cystine-modified TiO_2 visible-light photocatalyst, Res. Chem. Intermed. 41 (6) (2015) 3623–3636.
[19] H. Tang, D.u. Zhang, G. Tang, X. Ji, W. Li, C. Li, X. Yang, Hydrothermal synthesis and visible-light photocatalytic activity of α-Fe_2O_3/TiO_2 composite hollow microspheres, Ceram. Int. 39 (8) (2013) 8633–8640.
[20] S.-G. Kim, L.K. Dhandole, Y.-S. Seo, H.-S. Chung, W.-S. Chae, M. Cho, J.S. Jang, Active composite photocatalyst synthesized from inactive Rh & Sb doped TiO_2 nanorods: Enhanced degradation of organic pollutants & antibacterial activity under visible light irradiation, Appl. Catal. A: Gen. 564 (2018) 43–55.
[21] J. Zhong, F. Chen, J.L. Zhang, Carbon-Deposited TiO_2: Synthesis, Characterization, and Visible Photocatalytic Performance, J. Phys. Chem. C. 114 (2010) 933–939.
[22] J.-H. Tzeng, C.-H. Weng, Y.-H. Lin, S.-M. Huang, L.-T. Yen, J. Anotai, Y.-T. Lin, Synthesis, characterization, and visible light induced photoactivity of tourmaline-N-TiO_2 composite for photooxidation of ethylene, J. Ind. Eng. Chem. 80 (2019) 376–384.
[23] H. Wang, X. Yang, W. Xiong, Z. Zhang, Photocatalytic reduction of nitroarenes to azo compounds over N-doped TiO_2: relationship between catalysts and chemical reactivity, Res. Chem. Intermed. 41 (2013) 3981–3997.
[24] A. Abdelhaleem, W. Chu, X. Liang, Diphenamid degradation via sulfite activation under visible LED using Fe (III) impregnated N-doped TiO_2 photocatalyst, Appl. Catal. B: Environ. 244 (2019) 823–835.
[25] Y. Bai, H.Q. Sun, W.Q. Jin, Effects of pH values on the physicochemical properties and photocatalytic activities of nitrogen-doped TiO_2, J. Inorg. Mater. 23 (2008) 387–392.
[26] L.u. Xia, Y. Yang, Y. Cao, B. Liu, X. Li, X. Chen, H. Song, X. Zhang, B. Gao, J. Fu, Porous N-doped TiO_2 nanotubes arrays by reverse oxidation of TiN and their visible-light photocatalytic activity, Surf. Coat. Technol. 365 (2019) 237–241.
[27] Z. Luo, H. Jiang, D. Li, L. Hu, W. Geng, P. Wei, P. Ouyang, Improved photocatalytic activity and mechanism of Cu_2O/N-TiO_2 prepared by a two-step method, RSC Adv. 4 (2014) 17797.
[28] M. Kitano, K. Funatsu, M. Matsuoka, M. Ueshima, M. Anpo, Preparation of Nitrogen-Substituted TiO 2 Thin Film Photocatalysts by the Radio Frequency Magnetron Sputtering Deposition Method and Their Photocatalytic Reactivity under Visible Light Irradiation †, J. Phys. Chem. B 110 (50) (2006) 25266–25272.
[29] F. Dong, H. Wang, Z. Wu, J. Qiu, Marked enhancement of photocatalytic activity and photochemical stability of N–doped TiO_2 nanocrystals by Fe^{3+}/Fe^{2+} surface modification, J. Colloid Interface Sci. 343 (1) (2010) 200–208.
[30] K. Villa, A. Black, X. Domènech, J. Peral, Nitrogen doped TiO_2 for hydrogen production under visible light irradiation, Sol. Energy 86 (1) (2012) 558–566.
[31] X. Chen, X. Wang, Y. Hou, J. Huang, L. Wu, X. Fu, The effect of postnitridation annealing on the surface property and photocatalytic performance of N-doped TiO_2 under visible light irradiation, J. Catal. 255 (1) (2008) 59–67.
[32] Y. Shao, C. Cao, S. Chen, M. He, J. Fang, J. Chen, X. Li, D. Li, Investigation of nitrogen doped and carbon species decorated TiO_2 with enhanced visible light photocatalytic activity by using chitosan, Appl. Catal. B: Environ. 179 (2015) 344–351.
[33] H. Huang, Y. Song, N. Li, D. Chen, Q. Xu, H. Li, J. He, J. Lu, One-step in-situ preparation of N-doped TiO_2@C derived from Ti_3C_2 MXene for enhanced visible-light driven photodegradation, Appl. Catal. B: Environ. 251 (2019) 154–161.
[34] Q. Wang, H. Li, L. Chen, X. Huang, Monodispersed hard carbon spherules with uniform nanopores, Carbon 39 (14) (2001) 2211–2214.
[35] M. Waqas, S. Iqbal, A. Bahadur, A. Saeed, M. Raheel, M. Javed, Designing of a spatially separated hetero-junction pseudobrookite (Fe_2TiO_5-TiO_2) yolk-shell hollow spheres as efficient photocatalyst for water oxidation reaction, Appl. Catal. B: Environ. 219 (2017) 30–35.
[36] Q. Zeng, X. Xie, X. Wang, Y. Wang, G. Lu, D.Y.H. Pui, J. Sun, Enhanced photocatalytic performance of Ag@TiO_2 for the gaseous acetaldehyde photodegradation under fluorescent lamp, Chem. Eng. J. 341 (2018) 83–92.
[37] M. Bellardita, A. Di Paola, B. Megna, L. Palmisano, Determination of the crystallinity of TiO_2 photocatalysts, J. Photochem. Photobiol., A 367 (2018) 312–320.
[38] B. Wang, Q.Y. Chang, K. Gao, A hydrothermal reacting approach to prepare few-layer graphene from bulk graphite, Appl. Surf. Sci. 479 (2019) 20–24.
[39] J. Zhou, L. Zhao, Hypoxia-mimicking Co doped TiO_2 microporous coating on titanium with enhanced angiogenic and osteogenic activities, Acta Biomater. 43 (2016) 358–368.
[40] Q. Li, L. Zong, C. Li, J. Yang, Photocatalytic reduction of CO 2 on MgO/Ti_O 2 nanotube films, Appl. Surf. Sci. 314 (2014) 458–463.
[41] J. Ju, X.i. Chen, Y. Shi, J. Miao, D. Wu, Hydrothermal preparation and photocatalytic performance of N, S-doped nanometer TiO_2 under sunshine irradiation, Powder Technol. 237 (2013) 616–622.
[42] J. Senthilnathan, L. Philip, Photocatalytic degradation of lindane under UV and visible light using N-doped TiO_2, Chem. Eng. J. 161 (1-2) (2010) 83–92.
[43] F. Napoli, M. Chiesa, S. Livraghi, E. Giamello, S. Agnoli, G. Granozzi, G. Pacchioni, C. Di Valentin, The nitrogen photoactive centre in N-doped titanium dioxide formed via interaction of N atoms with the solid. Nature and energy level of the species, Chem. Phys. Lett. 477 (1-3) (2009) 135–138.
[44] A. Sanchez-Martinez, O. Ceballos-Sanchez, C. Koop-Santa, E.R. López-Mena, E. Orozco-Guareño, M. García-Guaderrama, N-doped TiO_2 nanoparticles obtained by a facile coprecipitation method at low temperature, Ceram. Int. 44 (5) (2018) 5273–5283.

[45] E.M. Samsudin, S.B. Abd Hamid, J.C. Juan, W.J. Basirun, A.E. Kandjani, S. K. Bhargava, Controlled nitrogen insertion in titanium dioxide for optimal photocatalytic degradation of atrazine, RSC Adv. 5 (55) (2015) 44041–44052.
[46] H. Irie, Y. Watanabe, K. Hashimoto, Nitrogen- Concentration Dependence on Photocatalytic Activity of $TiO_{2-x}N_x$ Powder, J. Phys. Chem. B. 107 (2003) 5483–5486.
[47] E.O. Oseghe, T.A.M. Msagati, B.B. Mamba, A.E. Ofomaja, An efficient and stable narrow bandgap carbon dot-brookite composite over other CD-TiO_2 polymorphs in rhodamine B degradation under LED light, Ceram. Int. 45 (11) (2019) 14173–14181.
[48] N. Fang, Y. Ding, C. Liu, Z. Chen, Effect of crystalline/amorphous structure on light absorption and carrier separationof CeO_2-TiO_2 heterojunctions, Appl. Surf. Sci. 452 (2018) 49–57.
[49] Z. Wang, W. Ma, C. Chen, H. Ji, J. Zhao, Probing paramagnetic species in titania-based heterogeneous photocatalysis by electron spin resonance (ESR) spectroscopy—A mini review, Chem. Eng. J. 170 (2-3) (2011) 353–362.
[50] M. Batzill, E.H. Morales, U. Diebold, Influence of nitrogen doping on the defect formation and surface properties of TiO_2 rutile and anatase, Phys. Rev. Lett. 96 (2006), 026103.
[51] S. Livraghi, M.C. Paganini, E. Giamello, A. Selloni, C. Di Valentin, G. Pacchioni, Origin of Photoactivity of Nitrogen-Doped Titanium Dioxide under Visible Light, J. Am. Chem. Soc. 128 (49) (2006) 15666–15671.
[52] C. Di Valentin, G. Pacchioni, A. Selloni, S. Livraghi, E. Giamello, Characterization of Paramagnetic Species in N-Doped TiO 2 Powders by EPR Spectroscopy and DFT Calculations, J. Phys. Chem. B 109 (23) (2005) 11414–11419.
[53] R. Asahi, T. Morikawa, Nitrogen complex species and its chemical nature in TiO_2 for visible-light sensitized photocatalysis, Chem. Phys. 339 (1-3) (2007) 57–63.
[54] J. Su, L. Zhu, G. Chen, Ultrasmall graphitic carbon nitride quantum dots decorated self-organized TiO_2 nanotube arrays with highly efficient photoelectrochemical activity, Appl. Catal. B: Environ. 186 (2016) 127–135.
[55] D. Wiedmer, E. Sagstuen, K. Welch, H.J. Haugen, H. Tiainen, Oxidative power of aqueous non-irradiated TiO_2-H_2O_2 suspensions: Methylene blue degradation and the role of reactive oxygen species, Appl. Catal. B: Environ. 198 (2016) 9–15.